

Tunable non-near-field focus and imaging of an unpolarized electromagnetic wave

Xiangdong Zhang

Department of Physics, Beijing Normal University, Beijing 100875, China

(Received 18 January 2005; revised manuscript received 29 March 2005; published 7 June 2005)

We propose a simple and efficient method to engineer absolute negative refraction for *both* polarizations of electromagnetic wave in two-dimensional photonic crystal by adding an additional component to the existing photonic crystal. The dielectric property of the additional component, as well as its insertion position in a unit cell, are chosen according to the field-energy distribution of Bloch states at the band edges. According to our design, the non-near-field focus and images for both polarized waves at the same structure and parameters, explicitly following the well-known wave-beam negative refraction law, can be realized.

DOI: 10.1103/PhysRevB.71.235103

PACS number(s): 78.20.Ci, 42.70.Qs, 41.20.Jb

I. INTRODUCTION

During the past few years, there has been a great deal of interest in studying the focus and imaging of electromagnetic waves based on the left-handed material (LHM) or two-dimensional (2D) photonic crystal (PC) flat lens.^{1–29} Ideally, such a lens can focus a point source on one side of the lens into a real point image on the other side even for the case of a parallel-sided slab of material.^{1,4} It possesses some advantages over conventional lenses. For example, it can break through the traditional limitation on lens performance and focus light on to an area smaller than a square wavelength. Recently, such image behaviors based on the LHM superlenses have been observed by some numerical simulations^{7–10} and experimental measurements.^{11–14} The 2D photonic-crystal-based flat lenses have also been designed and the images have also been observed in the near-field^{18–24} and non-near-field regions.^{25–29}

There are two aspects relating to the image. One is position (in near-field or non-near-field regions), and the other is resolution (full width at half maximum of the focus spot). The position of the image depends on the effective refractive index n of the sample and the homogeneity of the materials. For the case with $n=-1$ and single-mode transmission, the imaging behavior depends on the slab thickness and the object distance, explicitly following the well-known wave-beam negative refraction law as Refs. 27–29 had pointed out. However, due to the anisotropy of dispersion in some 2D PCs, the refraction angles are not linearly proportional to the incident angles when a plane wave is incident from vacuum to the PC. This is the reason why only the near-field images were observed in some works.^{18–24} The position of the image does not depend on whether or not the evanescent waves are amplified. That is to say, the focus and image can still be observed if only the propagating waves are considered. In such a case, the image resolution cannot beat the diffraction-limit. In contrast, the superlensing effect comes from the evanescent waves (or resonance transmission). The excitation of surface mode (or the appearance of resonant transmission) can improve the image resolution.^{22,29} This rule holds not only for the images in the near-field region, but also for the images in the non-near-field region.²⁹

It is well known that the electromagnetic (EM) wave can be decomposed into E polarization (S wave) and H polariza-

tion (P wave) modes for the 2D PC structures.^{24,28} However, the above discussions about the negative refraction and the focusing of the wave in the 2D PC all focused on a certain polarized wave, S wave or P wave. Recently, absolute negative refraction regions for *both* polarizations of electromagnetic wave in 2D PC with a square lattice have been found.²⁴ Thus, the focusing and image of unpolarized light have been realized by a microsuperlens consisting of such a PC (Ref. 24). However, due to the anisotropy of dispersion in 2D PC, such images only appear in the near-field region.²⁴ Thus, extensive applications of such a phenomenon are limited.

In this work, we present a method to engineer the absolute negative refraction by adding an additional component into the existing photonic crystal. The dielectric property of such a component, as well as its insertion position in a unit cell, are chosen according to the field-energy distribution of Bloch states at the band edges. According to such a method, the non-near-field focus and images for both polarized waves at the same structure and parameters, explicitly following the well-known wave-beam negative refraction law, can be realized.

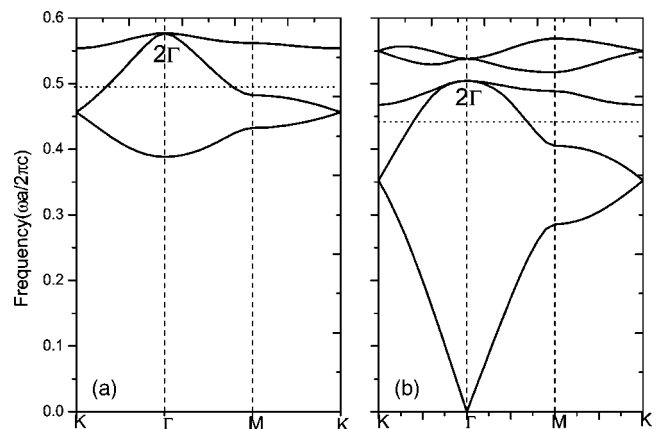


FIG. 1. The calculated photonic band structures of a triangular lattice of coated cylinder in air for (a) S wave and (b) P wave. The radii of the dielectric cylinder is $R=0.4a$. The inner metallic cylinders are $r=0.25a$ for both polarized waves. The dielectric constants are $\epsilon=12.96$. Dotted lines vs. the frequencies with negative refraction index of -1

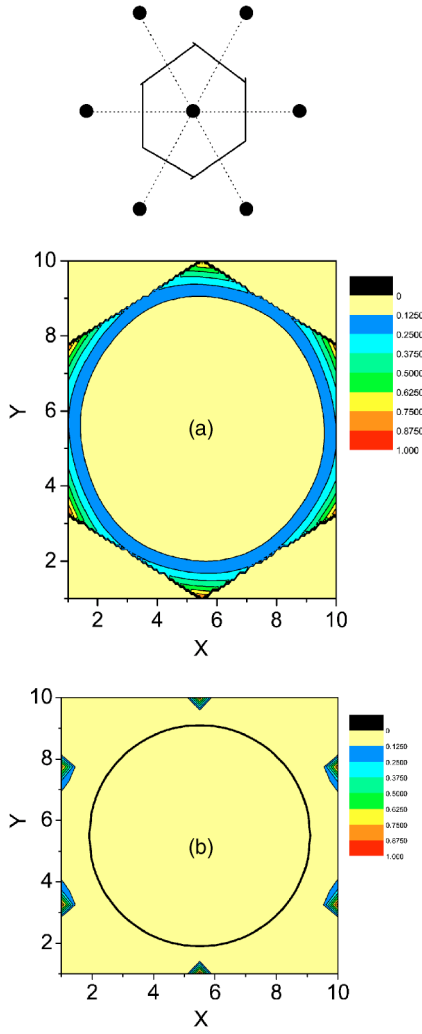


FIG. 2. (Color online) (a) The distribution of the absolute value of the electric field outside the cylinder (in arbitrary units) at the band edge 2Γ in the Wigner unit cell for the S wave. (b) The distribution of the absolute value of the displacement field outside the cylinder (in arbitrary units) at the band edge 2Γ in the Wigner unit cell for the P wave. The corresponding Wigner unit cell is plotted on the top of the figure.

This paper is arranged as follows. Our perturbative method to engineer negative refraction is described in Sec. II. In Sec. III, we design a flat lens to realize the non-near-field focus and images for both polarized waves at the same time. A conclusion is given in Sec. IV.

II. PERTURBATIVE METHOD TO ENGINEER NEGATIVE REFRACTION

We consider a two-dimensional triangular lattice of coated cylinders immersed in an air background with lattice constant $a=3$ mm. The coated cylinders have metallic cores coated with a dielectric coating. The radii of metallic core (r) and coated cylinder (R) are $0.25a$ and $0.4a$, respectively. The dielectric constants of dielectric coating are taken as 12.96 for both polarized waves. For the metallic component, we use the frequency dependent dielectric constant (Ref. 30),

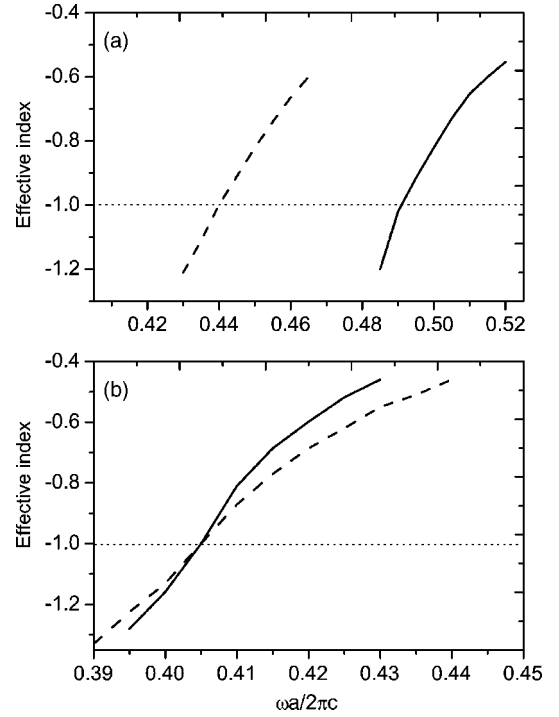


FIG. 3. Effective indexes vs frequencies (a) before and (b) after the additional components are inserted. The solid lines and dashed lines correspond to the S wave and P wave, respectively. The positions of relative refractive index of -1 are marked by dotted lines.

$\epsilon=1-f_p^2/f(f+i\gamma)$, where f_p and γ are the plasma frequency and the absorption coefficient. Following Ref. 30, for all numerical calculations carried out in this work, we have chosen $f_p=3600$ THz and $\gamma=340$ THz, which corresponds to a conductivity close to that of Ti. However, our discussion and conclusions given below can apply to other metal parameters as well. In order to simplify the problem, we first consider the cases without absorption ($\gamma=0$). The effect of absorption will be discussed at the latter part. The band structures of this system are calculated by the multiple-scattering Koringa-Kohn-Rostoker method.³¹ The results for the S and the P waves are plotted in Figs. 1(a) and 1(b), respectively.

Similar to the numerical simulations in Ref. 28, all-angle single-beam left-handed behaviors with relative refractive index of $n=-1$ for the S wave at $\omega=0.49(2\pi c/a)$ and the P wave at $\omega=0.44(2\pi c/a)$ have been found in this system. Dotted lines in Fig. 1(a) and 1(b) mark both of cases, respectively. However, we cannot find that the same structure and parameters yield $n=-1$ at the same frequency for both polarizations in this system.

In the following, we show that such a case can be realized by adding an additional component to the existing photonic crystal. The dielectric properties of such a component are chosen according to the field-energy distribution of Bloch states at the band edges. Thus, we calculate the field-energy distribution of band-edge state in a unit cell. For the 2Γ point of the S wave in Fig. 1(a), the absolute value of electric-field distribution outside the cylinder in a Wigner unit cell is plotted in Fig. 2(a). It is shown that the electric field $|E_{nk}(r)|$ at

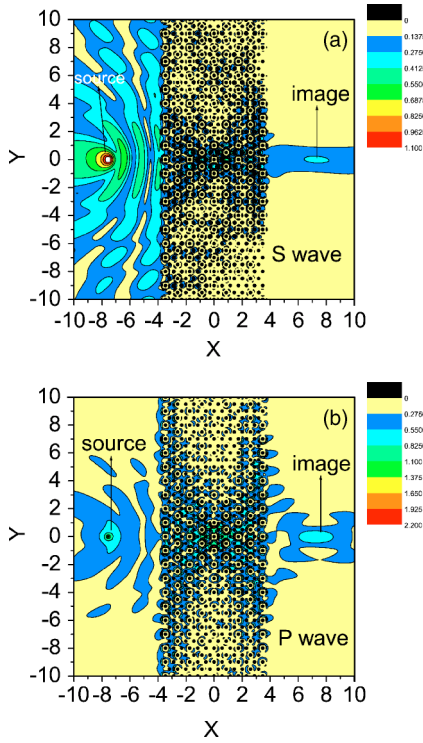


FIG. 4. (Color online) The intensity distributions of point sources and their images across a 2D photonic crystal slab with $7a$ thickness at frequency $\omega=0.405(2\pi c/a)$ for (a) S wave and (b) P wave. The parameters for cylinders are identical to those in Fig. 1.

six symmetric points of the Wigner unit cell are large. If we choose the dielectric materials to insert at the positions of these points, the field distribution in the unit cell will change, which leads to the shift of the band edge. The shift tendency and range for the S wave can be estimated by the following perturbation formula, which had been presented in our previous investigations:³¹

$$\left(\frac{\tilde{\omega}_{nk}}{\omega_{nk}}\right)^2 - 1 = \frac{\int [\tilde{\varepsilon}(r) - \varepsilon(r)] |E_{nk}(r)|^2 dr}{\int \varepsilon(r) |E_{nk}(r)|^2 dr}. \quad (1)$$

Here $\tilde{\varepsilon}(r)$ and $\tilde{\omega}_{nk}$ represent the new dielectric constant and eigenfrequency, respectively, corresponding to the original ε and ω_{nk} . The function $\tilde{\varepsilon}(r) - \varepsilon(r)$ is nonzero, only at the insertion position. The shift tendency and range of the band edge depend sensitively on the dielectric properties of the additional components as well as the field-energy distribution at the band edge. For example, if we choose the dielectric cylinders to insert, we can deduce that the band edge shifts down. With the change of the band structure, the negative refraction region will change at the same time.

Similar to the above case of the S wave, for the P wave, when the new components are inserted into the unit cell, the frequency shift can also be estimated by the following relation:³¹

$$\left(\frac{\tilde{\omega}_{nk}}{\omega_{nk}}\right)^2 - 1 = \frac{\int [\tilde{\varepsilon}^{-1}(r) - \varepsilon^{-1}(r)] |D_{nk}(r)|^2 dr}{\int \varepsilon^{-1}(r) |D_{nk}(r)|^2 dr}. \quad (2)$$

Here $D_{nk}(r)$ represents the displacement field in the unit cell. The intensity distribution of displacement field outside the cylinder in a Wigner unit cell at the 2Γ point of the P wave in Fig. 1(b) is plotted in Fig. 2(b). We find that the displacement field $|D_{nk}(r)|$ at six symmetric points of the Wigner unit cell are also large. If we choose the same dielectric components to insert the same positions in the unit cell for the P wave as the case of the S wave, the drop of the frequency at the 2Γ point can also be found. However, the shift extent for the P wave is smaller than that for the S wave. Therefore, it

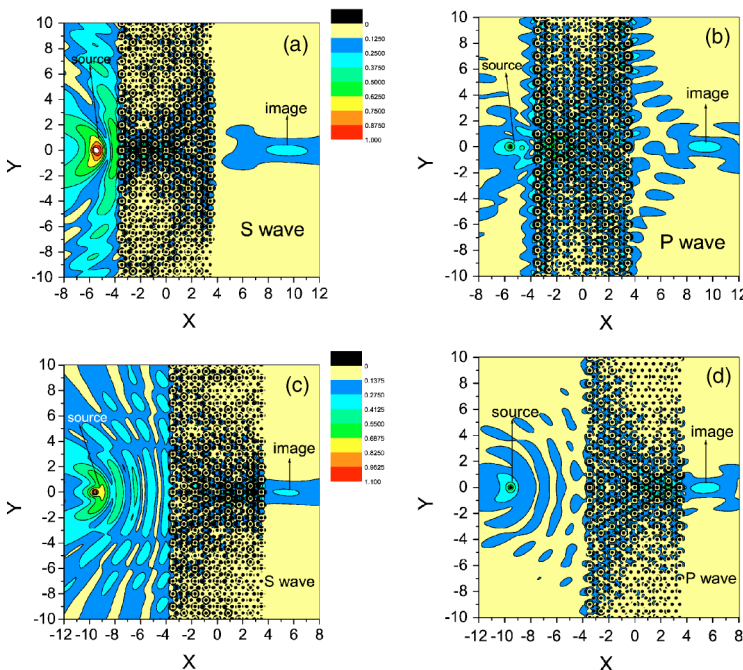


FIG. 5. (Color online) The intensity distributions of point sources and their images across a $7a$ 2D PC slab at frequency $\omega=0.405(2\pi c/a)$. (a) and (c) are for the S wave, (b) and (d) for the P wave. The point sources are placed at $2a$ and $9a$ from the left surface of the slab, respectively.

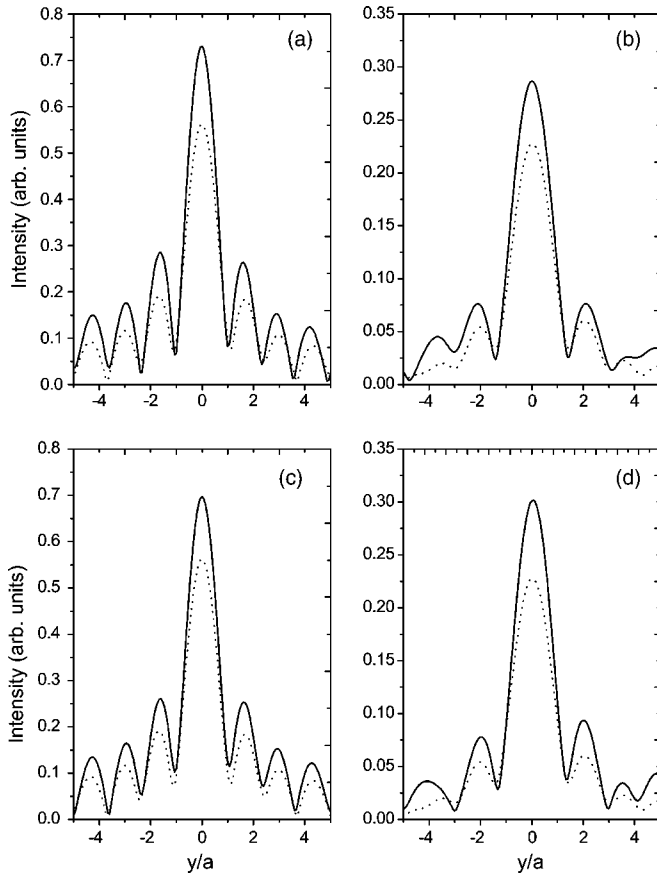


FIG. 6. Intensity distribution along the transverse (y) direction at the image plane. (a) and (b) correspond to the case for the S wave and P wave with absorption (dotted lines) and those without absorption (solid lines). (c) and (d) to the cases for the P wave and S wave with absorption (dotted lines) and those with absorption and gain (solid lines). The crystal and parameters are identical to those in Fig. 4.

is possible to obtain the same effective refractive index for both polarized waves through choosing suitable dielectric components to insert. For example, when the dielectric cylinders with $R=0.11a$ and $\epsilon=12.96$ are inserted, the frequency positions with relative refractive index of -1 become $\omega=0.405(2\pi c/a)$ for the S and P waves at the same time. That is to say, the same structure yields $n=-1$ at the same frequency for both polarized waves.

In order to demonstrate the above analysis, we do numerical simulations in the present systems. We take a slab sample with a $40a$ width and $10a$ thickness. The surface normal of the PC slab is along the ΓM direction. The parameters of coated cylinders are the same as the cases in Fig. 2. When a slit beam goes through the slab material, it will be refracted two times by two interfaces of the slab. There are different ray traces for the wave transmitting through the slab sample with various effective indexes, when the wave does not incident on the interface with normal direction. From the ray traces, we can deduce the effective refraction index of the slab material.²⁸

The calculated results of the negative refraction indexes as a function of the frequency are plotted in Figs. 3(a) and

3(b). Figures 3(a) and 3(b) correspond to the cases before and after the insertion, respectively. The solid lines correspond to the S wave and the dotted lines to the P wave. It is seen clearly that the positions of effective refractive index of $n=-1$ for the S and P waves in the original system are different. Comparing them with the estimated results from the equifrequency surface, we find that the agreements between them are well. However, the cross point of effective refractive indexes of $n=-1$ for the S and P waves appears at $\omega=0.405(2\pi c/a)$ after the dielectric cylinders with $R=0.11a$ and $\epsilon=12.96$ are inserted. This agrees with the perturbative approach.

III. NON-NEAR-FIELD IMAGE OF UNPOLARIZED ELECTROMAGNETIC WAVE

In the following, we design the flat lens to realize the far-field focusing and image of an unpolarized wave by using the above modulated PC system. We take a slab of the sample with $40a$ width and $7a$ thickness. A continuous-wave point source is placed at a distance $3.5a$ (half thickness of the sample) from the left surface of the slab. The frequency of the incident wave emitting from such a point source is $0.405(2\pi c/a)$, which corresponds to the case with relative refractive index of -1 for both polarized waves.

We employ the multiple-scattering method³¹ to calculate the propagation of both polarized waves in such a system. The typical results of E_z field pattern for the S wave and H_z field pattern for the P wave across the slab sample are plotted in Figs. 3(a) and 3(b), respectively. X and Y present the vertical and transverse directions of the wave propagating. The fields in the figures are over a $10a \times 10a$ region around the center of the sample. The geometries of the PC slab are also displayed. One can find quite a high quality image formed in the opposite side of the slab. A closer look at the data reveals that the transverse widths of the central peaks are about 1.05λ for the S wave and 0.8λ for the P wave. In particular, the positions of the images for both polarized waves are approximately the same. They are about at a distance of $3.5a$ from the right surface of the slab. That is to say, the image of the unpolarized wave point source can be realized by such a 2D PC slab. In order to clarify the sample thickness dependence of the image and focusing, we have also checked a series of slab samples with various thickness. Similar phenomena have also been observed.

In the following, we move the light source and see what happens to the imaging behavior. We first put a point source near the left surface of the slab, such as $2.0a$ from the left surface. The calculated intensity distributions for the S and P waves are plotted in Figs. 4(a) and 4(b), respectively. The images are found near $5a$ from the right surface. The corresponding results, that a point source is far from the left surface, are displayed in Figs. 4(c) and 4(d), respectively. In this case, the point source is placed at a distance of $5.0a$ from the left surface of the sample and the images are found near $2a$ from the right surface. That is to say, the images for both polarized waves obey fairly well the formula $A+B=L$ at the same time. Here A and B represent the object and image lengths, respectively, L is the thickness of the PC lens.

In the above calculations, we do not consider the effect of absorption. If we consider the effect of absorption and use the real dielectric constant ($\gamma=340$), our simulations show that the positions of the images do not change, except that the intensities of image peaks decrease for both polarized waves. For example, the transmission efficiency reduces 19% for the S wave and 20% for the P wave. It is interesting that the losses for both polarized waves can be overcome by introducing the same optical gain in the system. Figures 5(a) and 5(b) show the intensity distributions as a function of transverse coordinate (y/a) for the S wave and the P wave at the image plane, respectively. The solid lines correspond to the cases without absorption and the dotted lines to those with absorption. Comparing them, we find that the central peaks of the images decrease with the introducing of the absorption, which are in agreement with the previous results.^{24,28} The results, by introducing optical gain to remove the absorption for the corresponding case, are plotted in Figs. 5(c) and 5(d), respectively. The dotted lines in Figs. 5(c) and 5(d) are the same as those in Figs. 5(a) and 5(b). The solid lines are the results for the S and P waves with the dielectric constant $\epsilon=14-0.15i$ of the dielectric part of the coated cylinder, respectively. It is seen clearly that the losses by the absorption for both polarized waves have been overcome completely by introducing a small optical gain at the same time.

IV. SUMMARY AND CONCLUSION

In this work, we propose a simple and efficient method to engineer absolute negative refraction for *both* polarizations of electromagnetic wave in 2D PC by adding an additional component into the existing photonic crystal. The dielectric property of the additional component, as well as its insertion position in a unit cell, are chosen according to the field-energy distribution of the Bloch states at the band edges. Based on these, the flat lens has been designed, and the non-near-field focus and images for both polarized waves at the same structure and parameters, explicitly following the well-known wave-beam negative refraction law, have been realized. It is interesting that the losses by the absorption for both polarized waves can also be compensated by introducing a small optical gain at the same time.

ACKNOWLEDGMENTS

This work was supported by the National Natural Science Foundation of China (Grant No. 10374009) and the National Key Basic Research Special Foundation of China under Grants No. 2001CB610402 and 2004CB719804. The project is supported by NCET and the Grant from Beijing Normal University.

-
- ¹V. G. Veselago, Sov. Phys. Usp. **10**, 509 (1968).
²D. R. Smith, W. J. Padilla, D. C. Vier, S. C. Nemat-Nasser, and S. Schultz, Phys. Rev. Lett. **84**, 4184 (2000).
³R. A. Shelby, D. R. Smith, and S. Schultz, Science **292**, 77 (2001).
⁴J. B. Pendry, Phys. Rev. Lett. **85**, 3966 (2000).
⁵Opt. Express **11**, (7) (2003).
⁶G. Shvets, Phys. Rev. B **67**, 035109 (2003).
⁷V. A. Podolskiy, A. K. Sarychev, and V. M. Shalaev, Opt. Express **11**, 735 (2003).
⁸S. A. Ramakrishna and J. B. Pendry, Phys. Rev. B **67**, 201101(R) (2003).
⁹R. Merlin, Appl. Phys. Lett. **84**, 1290 (2004).
¹⁰L. Chen, S. He, and L. Shen, Phys. Rev. Lett. **92**, 107404 (2004).
¹¹D. R. Smith, D. Schurig, J. J. Mock, P. Kolinko, and P. Rye, Appl. Phys. Lett. **84**, 2244 (2004).
¹²Zhaowei Liu, Nicholas Fang, Ta-Jen Yen, and Xiang Zhang, Appl. Phys. Lett. **83**, 5184 (2003).
¹³A. Grbic and G. V. Eleftheriades, Phys. Rev. Lett. **92**, 117403 (2004).
¹⁴A. N. Lagarkov and V. N. Kissel, Phys. Rev. Lett. **92**, 077401 (2004).
¹⁵H. Kosaka, T. Kawashima, A. Tomita, M. Notomi, T. Tamamura, T. Sato, and S. Kawakami, Phys. Rev. B **58**, R10096 (1998).
¹⁶M. Notomi, Phys. Rev. B **62**, 10696 (2000).
¹⁷B. Gralak, S. Enoch, and G. Tayeb, J. Opt. Soc. Am. A **17**, 1012 (2000).
¹⁸C. Luo, S. G. Johnson, J. D. Joannopoulos, and J. B. Pendry, Phys. Rev. B **65**, 201104(R) (2002).
¹⁹E. Cubukcu, K. Aydin, E. Ozbay, S. Foteinopoulou, and C. M. Soukoulis, Nature (London) **423**, 604 (2003).
²⁰P. V. Parimi, W. T. Lu, P. Vodo, and S. Sridhar, Nature (London) **426**, 404 (2003).
²¹E. Cubukcu, K. Aydin, E. Ozbay, S. Foteinopoulou, and C. M. Soukoulis, Phys. Rev. Lett. **91**, 207401 (2003).
²²C. Luo, S. G. Johnson, J. D. Joannopoulos, and J. B. Pendry, Phys. Rev. B **68**, 045115 (2003).
²³Z. Y. Li and L. L. Lin, Phys. Rev. B **68**, 245110 (2003).
²⁴X. Zhang, Phys. Rev. B **70**, 205102 (2004); Appl. Phys. Lett. **86**, 121103 (2005).
²⁵X. Wang, Z. F. Ren, and K. Kempa, Opt. Express **12**, 2919 (2004).
²⁶A. Berrier, M. Mulot, M. Swillo, M. Qiu, L. Thylen, A. Talneau, and S. Anand, Phys. Rev. Lett. **93**, 073902 (2004).
²⁷X. Hu and C. T. Chan, Appl. Phys. Lett. **85**, 1520 (2004).
²⁸X. Zhang, Phys. Rev. B **70**, 195110 (2004); Phys. Rev. E **71**, 037601 (2005).
²⁹X. Zhang, Phys. Rev. B **71**, 165116 (2005).
³⁰L. M. Li, Z. Q. Zhang and X. Zhang, Phys. Rev. B **58**, 15589 (1998); M. M. Sigalas, C. T. Chan, K. M. Ho, and C. M. Soukoulis, *ibid.* **52**, 11744 (1995).
³¹X. Zhang, Z. Q. Zhang, L. M. Li, C. Jin, D. Zhang, B. Man, and B. Cheng, Phys. Rev. B **61**, 1892 (2000); X. Zhang and Z. Q. Zhang, *ibid.* **61**, 9847 (2000).